HHS Public Access

Author manuscript

Cell Chem Biol. Author manuscript; available in PMC 2020 November 21.

Published in final edited form as:

Cell Chem Biol. 2019 November 21; 26(11): 1586–1593.e3. doi:10.1016/j.chembiol.2019.08.008.

Amidino-Rocaglates – A potent class of eIF4A inhibitors

Jennifer Chu[1], **Wenhan Zhang**[2], **Regina Cencic**[1], **William G. Devine**[2], **Dmitri Beglov**[3], **Thomas Henkel**[5], **Lauren E. Brown**[2,4], **Sandor Vadja**[2,3], **John A. Porco Jr.**[2,4,*], **Jerry Pelletier**[1,6,7,*]

[1]Department of Biochemistry, McGill University, Montreal, Canada

[2]Department of Chemistry, Boston University, MA, USA

[3]Department of Biomedical Engineering, Boston University, MA, USA

[4]Center for Molecular Discovery (BU-CMD), Boston University, MA, USA

[5]IMAX Discovery GmbH, Dortmund, Germany

[6]Department of Oncology, McGill University, Montreal, Canada

[7]Rosalind & Morris Goodman Cancer Research Centre, McGill University, Montreal, Canada

Summary.

Rocaglates share a common cyclopentabenzo[*b*]furan core that inhibit eukaryotic translation initiation by modifying the behaviour of the RNA helicase, eIF4A. Working as interfacial inhibitors, rocaglates stabilize the association between eIF4A and RNA which can lead to the formation of steric barriers that block initiating ribosomes. There is significant interest in the development and expansion of rocaglate derivatives as several members of this family have been shown to possess potent anti-neoplastic activity *in vitro* and *in vivo*. To further our understanding of rocaglate diversity and drug design, herein we explore the RNA clamping activity of >200 unique rocaglate derivatives. Through this, we report on the identification and characterization of a potent class of synthetic rocaglates called amidino-rocaglates. These compounds are among the most potent rocaglates documented to date, and taken together, this work offers important information that will guide the future design of rocaglates with improved biological properties.

[*]To whom correspondences should be addressed: Jerry Pelletier (Lead Contact), Department of Biochemistry, McGill University, Montreal, Quebec, H3G 1Y6, Canada. Tel: 1-514-398-2323; jerry.pelletier@mcgill.ca, John A. Porco Jr., Department of Chemistry and Center for Molecular Discovery (BU-CMD), 590 Commonwealth Ave., Boston University, Boston, MA 02215. Tel: 1-617-353-2493; porco@bu.edu.

Author Contributions

J.C., W.Z., J.A.P. Jr, and J.P. conceived and designed this study. J.C., W.Z., R.C., W.G.D., D.B., L.E.B., and S.V. acquired, analyzed, and interpreted data. T.H. provided essential reagents. J.C. and J.P. wrote the manuscript. All authors commented on, edited and approved the manuscript.

Lead Contact: J Pelletier

Declaration of Interests

J.C., W.Z., J.A.P. Jr, and J.P. have filed a US provisional patent application on the use of amidino-and amino-rocaglates as potent translation inhibitors and anticancer agents.

Data and Code Availability

This study did not generate/analyze datasets/code.

Graphical Abstract

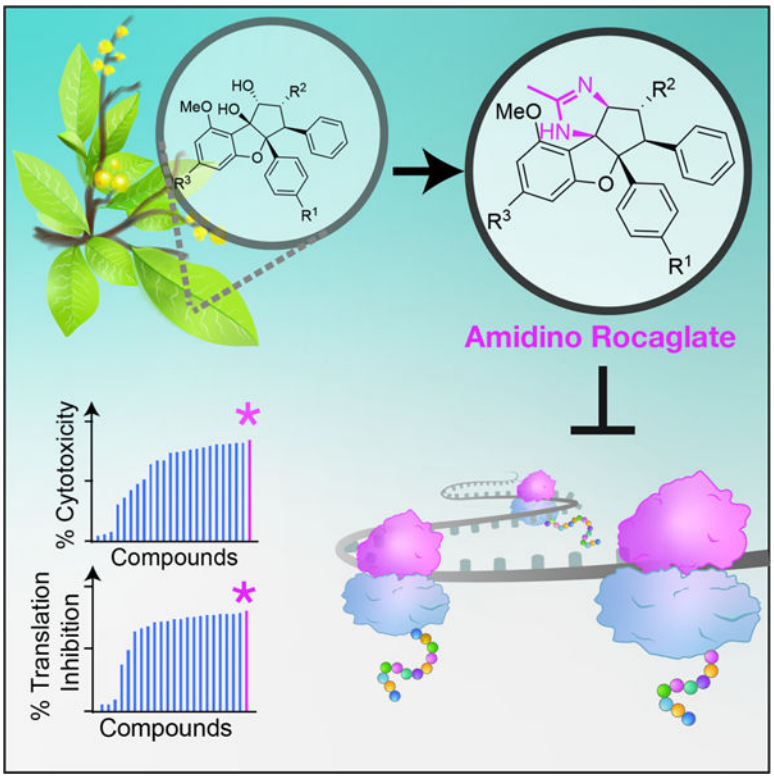

eTOC

A screen of >200 rocaglates identified a novel, potent chemical series, amidino-rocaglates, that target eIF4A1 and eIF4A2 to potently inhibit translation, tumor cell viability, and are effective in synergizing with DNA damaging agents *in vivo* against MYC-driven lymphomas. These compounds are promising anti-cancer agents.

Keywords

amidino-rocaglates; eIF4A; eIF4F; translation initiation; interfacial inhibitor

Introduction

Small molecules targeting the translation machinery show considerable promise in the treatment of a variety of human maladies including cancer, viral infection, and neurodegeneration. In particular, there is significant interest towards the development of a family of compounds collectively known as rocaglates (Bhat et al., 2015). Rocaglates are a class of translation inhibitors that possess potent cytotoxic activity against tumor cells (Bhat et al., 2015). This family of small molecules shares a common cyclopenta[*b*]benzofuran core and were originally isolated from extracts of the *Aglaia* species of angiosperms (King et al., 1982). To date, numerous rocaglate analogs have been synthesized with the goals of improving potency and bioavailability (Ebada et al., 2011; Pan et al., 2014; Ribeiro et al.,

2012). Studies using silvestrol, a natural product isolated from *Aglaia foveolata*, indicate that rocaglates enhance the RNA binding affinity of the DEAD-box RNA helicase, eukaryotic initiation factor (eIF) 4A (Bordeleau et al., 2008; Iwasaki et al., 2016).

Cap-dependent translation is regulated by the rate-limiting eIF4F complex which recognizes mRNA cap structures *via* its eIF4E subunit, remodels adjacent mRNA structure via eIF4A, and recruits 43S pre-initiation complexes (40S subunit and associated factors) through its eIF4G subunit (Pelletier and Sonenberg, 2019). The dependency on eIF4F for ribosome recruitment by different mRNAs varies and scales with the degree of 5' leader secondary structure (Svitkin et al., 2001). Only ~5% of eIF4A is present in the eIF4F complex, suggesting that multiple eIF4A molecules may be used per initiation round and/or eIF4A may have non-eIF4F related activities in translation (Sokabe and Fraser, 2017). Assembly of the eIF4F complex is under mTOR regulation, ensuring that rheostatic and selective regulation of mRNA translation is linked to extra- and intra-cellular cues (Pelletier and Sonenberg, 2019).

Structural elucidation of a rocaglate[RocA]:eIF4A1:polypurine RNA complex revealed that rocaglates function as interfacial inhibitors and make critical contacts with eIF4A1 (F163L, Q195) and two adjacent RNA purine bases (Iwasaki et al., 2019). When present within 5' mRNA leader regions, polypurine sequences serve as nucleation sites for rocaglate:eIF4A1 complexes, leading to the formation of steric barriers that impede 43S PIC scanning (Iwasaki et al., 2016). A rocaglate-resistant eIF4A1 mutant (F163L) has been characterized and introduction of this allele into cells using CRISPR/Cas9-mediated gene editing confers resistance to rocaglate cytotoxicity (Chu et al., 2016; Iwasaki et al., 2019), further demonstrating that the mechanism of action of these compounds is dependent on their ability to interfere with eIF4A1 activity. Mammalian cells also express a second eIF4A paralog (known as eIF4A2) that shares 90% amino acid identity with eIF4A1 and has been shown to participate in translation initiation (Rogers et al., 2002; Yoder-Hill et al., 1993). However, the effects of rocaglates on eIF4A2 have been largely unexplored as eIF4A1 is the predominant paralog in most cell types (Galicia-Vazquez et al., 2012; Nielsen and Trachsel, 1988).

Interest in rocaglates as potential anti-neoplastic agents and the significant efforts made towards the development of synthetic strategies have greatly expanded the number of members in this family (Qian et al., 2016). Herein, we characterized the activity of >200 rocaglates from an in-house library (the BU-CMD collection) to induce RNA clamping of eIF4A1 and eIF4A2. During the course of these studies, we uncovered and characterized amidino-rocaglates (ADRs) that rank among the most potent synthetic derivatives identified to date.

Results and Discussion

Rocaglates similarly enhance RNA binding of eIF4A1 and eIF4A2.

In order to rapidly evaluate the ability of rocaglates to stimulate binding of eIF4A to RNA, we took advantage of a fluorescence polarization (FP) assay using a FAM (fluorescein amidite)-labelled RNA probe (Fig 1a) (Iwasaki et al., 2016). The ATPase activity of eIF4A1

is stimulated by the presence of RNA; previous studies have documented that the homoribopolymers poly r(A) and poly r(U) are more potent than poly r(C), poly r(I), poly r(G), globin mRNA, tRNA, poly r(I-C), or poly r(A)•poly r(U) substrates, suggesting that eIF4A1 has an inherent nucleotide bias for RNA binding (Abramson et al., 1987). Using the FP assay, we revisited the RNA sequence specificity of eIF4A1, and took the opportunity to characterize the RNA binding activity of its paralog, eIF4A2. Studies focusing on the pharmacological targeting of eIF4A2 have been comparatively limited due to the fact that it is the less abundant eIF4A variant in many cell types. However, this remains an area of interest to explore as there is evidence suggesting that eIF4A2 may have tumor promoting effects (Chen et al., 2019) and in certain cancers, eIF4A2 is the predominant paralog (Wolfe et al., 2014). The ability to target eIF4A2 is also important within the context of eIF4A1 inhibition as it has been demonstrated that suppression of eIF4A1 leads to increased eIF4A2 expression (Galicia-Vazquez et al., 2012). We found that both proteins have a preference for mixed polypurine (poly r$(AG)_8$ or poly rA$(GAA)_5$) sequences versus poly r$(A)_{16}$, poly r$(C)_{16}$ or mixed polypyrimidine (poly r$(UC)_8$) (Figs 1b, c). In the presence of the synthetic rocaglate, CR-1–31-B, the binding activities of eIF4A1 and eIF4A2 to poly r$(AG)_8$ were enhanced to similar extents, indicating that the compound targets both paralogs equally (Fig 1d, e).

The rocaglate hydroxamate CR-1–31-B also preferentially stimulated binding of eIF4A1 to poly rA$(GAA)_5$ and to a lesser extent poly $(A)_{16}$, but had no effect when a polypyrimidine-containing RNA (poly r$(C)_{16}$ or poly r$(UC)_8$) was used (Fig 1f). To better understand the requirements for rocaglate-mediated stimulation of RNA binding, we next performed this experiment using RNA probes with varying (AG) repeat length. A single r(AG) dinucleotide embedded within a polypyrimidine track was sufficient for CR-1–31-B to stimulate eIF4A1-RNA binding and the extent of binding increased with higher AG content (Fig 1g). The location of an AG dinucleotide within a 16 nt RNA probe harboring otherwise poly r(U) sequences influenced stimulation of RNA binding, with the optimal preference being seven nucleotides downstream from the RNA 5’ end (Fig S1). Taken together, these results indicate that: (i) eIF4A1 and eIF4A2 show similar RNA sequence binding specificity and have a distinct preference towards polypurine bases, (ii) the RNA binding activity of both eIF4A1 and eIF4A2 is similarly stimulated by CR-1–31-B, and (iii) the stimulation of RNA binding of eIF4A1 to RNA by CR-1–31-B scales with polypurine content.

Comparative assessment of rocaglate-induced eIF4A:RNA binding.

The interest towards rocaglates as potential anti-neoplastic agents and the significant efforts made towards the development of synthetic strategies have greatly expanded the number of members in this family (Qian et al., 2016). However, it has also meant that various laboratories are employing different rocaglates in biological studies. These include the natural products, silvestrol and RocA, as well as the synthetic derivatives CR-1–31-B, SDS-1–021, RHT, and FL3 (Figs. 1d, 2a). The *X*-ray crystal structure of eIF4A1 complexed with RocA and poly r$(AG)_5$ RNA revealed that aryl rings A and B (Fig 2a) stack with adjacent adenine and guanine bases, respectively (Iwasaki et al., 2019). In addition, the *C*8b-OH hydrogen bonds to the *N7* of the same guanine stacked to aryl ring B. One outstanding question is whether structural differences among rocaglates can influence polypurine

sequence preference. To address this, we took advantage of an in-house curated library of >200 rocaglates (which are part of the BU-CMD collection) to rank compounds for their ability to stimulate eIF4A1:RNA binding (Fig 2b, Table S1). We were also interested to see if there were any rocaglate capable of imparting a polypyrimidine [poly r$(UC)_8$] specificity to eIF4A1 but found that none of the compounds in our collection possessed this property (Fig 2b). We also did not identify any rocaglate that significantly stimulated RNA binding to eIF4A1 over eIF4A2 or vice versa (Fig 2c, Table S1). This is perhaps not surprising since the two amino acids involved in rocaglate binding (F163 [F164 in eIF4A2] and Q195 [Q196 in eIF4A2]) are conserved between the two proteins. A significant proportion of compounds stimulated binding of poly r$(AG)_8$ RNA to both eIF4A1 and eIF4A2 (Fig 2c, Table S1).

ADRs represent a class of potent rocaglates.

Among the most potent inhibitors of translation uncovered by our screen were two ADRs, CMLD012072 and CMLD012073 (Fig 2b). These arose as a consequence of a recently described intercepted retro-Nazarov reaction (Zhang et al., 2019). The ADRs are distinguished from other rocaglates by the presence of an additional heterocyclic ring (imidazoline) which is fused to the cyclopenta[*b*]benzofuran core (Fig 2b). In *in vitro* translation assays, CMLD012073 was ~3-fold more potent at inhibiting cap-dependent translation (FF) than CR-1–31-B (Fig 2d). In ribosome recruitment experiments, CMLD012073 (and CR-1–31-B) inhibited assembly of the 80S ribosome on the mRNA, thus further supporting the notion that this compound acts as an inhibitor of initiation (Fig 2e).

To characterize this chemical series, we synthesized 21 additional congeners and determined their relative potency towards inhibiting translation *in vitro* and cellular cytotoxicity (Fig 3a and Table S2). Amongst these was CMLD012612, an ADR containing a hydroxamate group, which we found to be the most potent analogue (Fig 3a, b). We have previously demonstrated that the addition of the hydroxamate moiety improves rocaglate potency (Roche et al., 2010; Rodrigo et al., 2012). Compounds containing this moiety (eg. CR-1–31-B, RHT, and SDS-1–0-21) ranked highly among all rocaglates in our collection with respect to enhancing eIF4A1:RNA binding (Fig 2b). To understand how the imidazoline modification present in the amidino-rocaglates impacts binding in the context of available structural data, CMLD012612 was computationally modeled into the 5ZC9 structure (Fig 3c). The modeled pose shows stacking of aryl rings A and B with RNA base A7 and G8, respectively. Interactions with eIF4A1 F163 is mediated by ring C and with Q195 by the *C*1-OH and *C*2 carbonyl. We observed a potential hydrogen bond interaction (2.4 Å) between the imidazoline N-H (shown in white) and *N*7 of G8. This interaction is reminiscent of the hydrogen bond between *N*7 of G8 and the *C*8b-OH of RocA, previously attributed as a main driver of purine-selectivity (Iwasaki et al., 2019).

To establish initial structure activity relationships (SAR) for amidino rocaglates (ADRs), we compared IC_{50}'s of compounds against NIH/3T3 cells (Fig 3a). We noticed increased cytotoxicity with a decrease in the rigidity and size of the imidazoline substituent (Fig 3d, red). In particular, an ADR (CMLD012073) bearing a methyl (Me) group exhibited an IC_{50} of 10 nM. Subsequently, we evaluated substitution of the ADR carbonyl moiety (blue) where

we found increased cytotoxicity of the electron-rich carbonyls (Fig 3d, NMe(OMe) > NMe_2 > OMe > Me > H). Of note, the stereochemistry of ADRs is also critical for biological activity, where we found significantly reduced cytotoxicity (IC_{50} = 454 nM) for the unsaturated aldehyde CMLD012607. The latter trends appear to correlate with the strong ability of the hydroxamate residue of CMLD012612 to act as hydrogen bond acceptor to the Q195 residue of eIF4A (Fig 3c) (Iwasaki et al., 2019; Rodrigo et al., 2012; Tecle et al., 2009).

The activity of CMLD012612 surpasses those of our previous lead compounds, CR-1–31-B and CMLD012073, with respect to inhibition of cellular translation (Fig 4a), and cytotoxicity towards NIH/3T3 cells (Fig 4b; IC_{50} ~ 2 nM). This cytotoxicity was significantly blunted in $eIF4A1^{em1JP}$ cells, a CRISPR-engineered NIH/3T3 line harboring rocaglate-resistant eIF4A1(F163L) alleles (Fig 4b and Table S2), demonstrating that the mechanism of action of CMLD012612 is eIF4A1 dependent.

Rocaglates are capable of sensitizing drug-resistant tumors to front-line and targeted therapies (eg, doxorubicin, dexamethasone, vemurafenib) (Boussemart et al., 2014; Robert et al., 2014; Rodrigo et al., 2012)(Bordeleau et al., 2008). This was first shown with doxoribucin in the Em-Myc model (Bordeleau et al., 2008), an *in vivo* tumor model that recapitulates many pathological features observed in Non-Hodgkin lymphomas. Dysregulation of mTOR signaling (through inactivation of Pten or sustained Akt activity) in this model accelerates tumor onset, suppresses apoptosis, and confers resistance towards conventional chemotherapies such as cyclophosphamide and doxorubicin (Wendel et al., 2004). As well, suppression of eIF4F is capable of restoring chemosensitivity through blunting of pro-survival signals (Wendel et al., 2004). To characterize the *in vivo* activity of CMLD012612, we first assessed the ability of the compound to inhibit translation following intraperitoneal delivery. CMLD012612, like CR-1–31-B, effectively suppressed liver polysomes 3 h after injection indicating inhibitory activity towards protein synthesis (Fig 4c). When administered to mice bearing myr-Akt/*E*μ-*Myc* lymphomas, CMLD012612 effectively synergized with doxorubicin leading to complete tumor loss that extended to 15–16 days (Fig. 4d).

Our large-scale screen has identified a potent class of rocaglates – the ADRs. This screen has also guided us in the design of an ADR derivative, CMLD012612, which was found to be more potent than previous lead compounds. Whereas the IC_{50} of CR-1–31-B towards NIH/3T3 cells is ~8.5 nM, CMLD012612 displays an IC_{50} of ~2 nM (Fig 4b). The primary mechanism of action of CMLD012612 is dependent on eIF4A1, since $eIF4A^{em1jp}$ cells are at least 10-fold more resistant than parental NIH/3T3 cells. The sensitivity of $eIF4A^{em1jp}$ cells to CMLD012612 observed at higher concentrations may be due to the presence of wild-type eIF4A2 in the cells. Our results highlight the value of further exploring modification of the rocaglate core including the *C*8b position for improving and extending the potency of rocaglates, while retaining *in vivo* activity. Taken together, these results identify ADRs as a potent subclass of inhibitors capable of targeting eIF4A-mediated initiation *in vitro* and *in vivo*.

STAR Methods

Lead Contact and Materials Availability

Further information and requests for resources and reagents should be directed to and will be fulfilled by Jerry Pelletier (Lead Contact) (jerry.pelletier@mcgill.ca) or John A. Porco, Jr. (porco@bu.edu).

Experimental Model and Subject Details

All cell lines used in this study were maintained in DMEM supplemented with 10% FBS (Wisent), 100 U/mL penicillin/streptomycin, and 2 mM L-glutamine at 37 °C and 5% CO_2. Animal studies were approved by the McGill University Faculty of Medicine Animal Care Committee. All mice used in this study were female C57BL/6 mice, aged 6–8 weeks.

Method Details

Compounds.—Rocaglate derivatives provided from the BU-CMD collection were synthesized using ESIPT photocycloaddition of 3-hydroxyflavones with cinnamates as previously published followed by further functionalizations [15–17]. Note that there are duplicate values for some compounds in this collection from different synthesis batches or containing two enantiomers (see Table S1). Compounds were resuspended to 10 mM in neat DMSO and stored at −80° C.

Purification of Recombinant Proteins.—BL21 (DE3) *E. coli* cells were transformed with pET15b-His_6-eIF4A1 or pET15b-His_6-eIF4A2 plasmids. Single colonies were picked and grown in an overnight starter culture at 37 °C in LB media supplemented with 100 mg/L ampicillin. On the following day, the starter culture was used to inoculate at a 1:50 dilution, and the cultures continued growing at 37 °C. When the OD_{600} reached 0.6–0.8, 1 mM IPTG was added to induce protein production and the cultures were grown for an additional 3 h. Cells were pelleted, resuspended in a buffer containing 20 mM Tris (pH 7.5), 10% glycerol, 0.1 mM EDTA, 200 mM KCl, 0.1% Triton X-100, 3.4 mM β-mercaptoethanol, and sonicated. The lysates were cleared via centrifugation and supplemented with 20 mM imidazole prior to loading onto a Ni-NTA agarose column (Qiagen). The column was washed 3 times with 4 column volumes of wash buffer 1 (20 mM Tris (pH 7.5), 10% glycerol, 0.1 mM EDTA, 800 mM KCl, 20 mM imidazole), and then washed 3 more times with 4 column volumes of wash buffer 2 (Wash buffer 1 containing 300 mM KCl). Elution was achieved using Wash buffer 2 supplemented with 200 mM imidazole and dialyzed overnight in a buffer containing 20 mM Tris (pH 7.5), 10% glycerol, 0.1 mM EDTA, 100 mM KCl, and 2 mM DTT. The resulting samples were further purified using a Q-Sepharose Fast Flow (Amersham) column and eluted with a 100 – 500 mM KCl gradient in 20 mM Tris (pH 7.5,) 10% glycrerol and 0.1 mM EDTA. Eluted fractions of high protein yield and purity (as assessed by Coomassie blue staining) were combined and dialyzed against 20 mM Tris (pH 7.5), 10% glycerol, 0.1 mM EDTA and 2 mM DTT.

In Vitro* Translation Assays.—In vitro* translation assays performed in Krebs-2 cell extracts supplemented with 5 mM $MgCl_2$, 30 mM Tris-HCl (pH 7.5), 1.5 mM ATP, 0.1 mM GTP, 0.6 mM CTP, 10 mM dipotassium creatine phosphate, 80 μg/mL creatine kinase, and

0.04 mM amino acids. The specified mRNA reporters were added to each reaction at a final concentration of 10 ng/μL. Translation reactions were performed in the presence or absence of compound for 60 minutes at 30 °C prior to the measurement of luciferase activities.

Fluorescence Polarization Assays.—Unless otherwise specified, eIF4A (500 nM) was incubated with 10 nM FAM-labelled RNA for 30 min in FP buffer (14.4 mM HEPES-NaOH (pH 8), 108 mM NaCl, 1 mM $MgCl_2$, 14.4% glycerol, 0.1% DMSO, 2 mM DTT, 1 mM AMPPNP) at room temperature in black, low volume 384 well plates (Corning 3820). FP readings were performed on a Pherastar FS microplate reader (BMG Labtech).

Sulforhodamine B (SRB) assay.—NIH/3T3 cells were seeded at a density of 1000 cells/well in a 96 well format and incubated in presence of 40 nM compound. After 4 days of culture, cells were washed with PBS, fixed with 50% trichloroacetic (TCA) acid for 1 hour, and stained with 0.5% sulforhodamine B in 1% acetic acid for 15 min. Plates were then washed 5 times with 1% acetic acid, dried, and the stained wells were resuspended with 10 mM Tris (pH 9) prior to measuring the absorbance at 510 nm on a Spectramax M5 (Molecular Devices).

[^{35}S]-Methionine Labeling.—293T cells were seeded at a density of 40 000 cells per well in a 24 well plate and on the following day incubated in the presence of the indicated concentration of compound in methionine/cysteine free media supplemented with 10% dialyzed FBS for 1 hour. *De novo* protein synthesis was monitored through the addition of S^{35}methionine/cysteine labelling mix (1175 Ci/mmol) and incubating the cells for an additional 15 min. The labeling reaction was terminated by washing the cells twice with ice cold PBS and lysing with RIPA buffer. Half of the lysate was then spotted onto 3 MM Whatman paper that had been pre-blocked with amino acids and precipitated using 10% trichloroacetic acid (TCA) at 4 °C for 20 min. The spotted samples were boiled in 5% TCA for 15 min, washed twice with 5% TCA, followed by one wash with 75% EtOH, dried, and quantitated using scintillation counting. Protein concentration was determined with the DC Protein assay (BioRad) and used for normalization.

Ribosome binding assays.—^{32}P-labeled $(AG)_{10}$-FF/HCV/Ren mRNA was incubated with 100 nM eIF4A1 in the presence of 500 nM compound for 10 min at RT, then added to rabbit reticulocyte lysates in the presence of 600 μM cycloheximide. Incubations were performed at 30 °C for 10 min after which time, the lysate was applied onto a 10–30% glycerol gradient. Centrifugation was for 3.5 h at 39,000 rpm at 4 °C in an SW40 rotor. Fractions were collected using a Brandel Tube Peircer connected to an ISCO fraction collector and radioactivity was determined by scintillation counting.

Liver polysomes.—For polysome profiling analysis on liver extracts, female C57BL/6 mice were treated at a single dose of either vehicle (5.2% PEG400/5.2% Tween-80), 0.2 mg/kg CR-1–31-B or 0.5 mg/kg CMLD012612 and animals sacrificed 3 h after injection. Livers were excised, washed in cold PBS containing 100 μg/mL cycloheximide and homogenized in 3 volumes of lysis buffer (40 mM HEPES (pH 7.5), 100 μM KCl, 5 mM $MgCl_2$, 100 mg/mL cycloheximide) in a Eurostar Power-b homogenizer (IKA Liver

Labortechnik, Staufen, Germany). After homogenization, samples were centrifuged for 10 min at 1200 × *g* and 4 °C and the supernatant transferred to a new tube.

Three hundred microliter of detergent mix (0.5% Triton X-100 and 0.5% sodium deoxycholate) were added to 150 μl of supernatant and the sample spun briefly (10,000 × g for 10 min) before loading onto 10–50% sucrose gradients and centrifuged in an SW40 rotor at 35 000 rpm for 135 min. Gradients were analyzed by piercing the tube with a Brandel tube piercer and passing 60% sucrose through the bottom of the tube. Recording of the data was performed using InstaCal Version 5.70 and TracerDaq Version 1.9.0.0 (Measurement Computing Corporation, Norton, MA).

Lymphoma Studies.—A total of 2×10^6 Eμ-Myc/myr-Akt lymphoma cells were injected into the tail vein of 6 – 8 week-old female C57BL/6 mice. Upon development of well-palpable tumors (auxiliary and inguinal lymph nodes), mice were injected intraperitoneal (IP) with doxorubicin (once at 10 mg/kg) or CMLD012612 (0.2 mg/kg daily for 5 days). In combination studies, CMLD012612 was administered once daily for 5 consecutive days, while doxorubicin was administered on day 2. Tumor-free survival is defined as the time between disappearance and reappearance of a palpable lymphoma following treatment.

Quantification and Statistical Analysis

All values reported in this study represent the mean ± SEM of at least 3 biological replicates. The IC_{50} values for *in vitro* translation in Krebs extracts and cell viability were determined from 3–5 independent experiments using 6 concentration points and were fitted using nonlinear regression on Graphpad Prism 7.0c.

Supplementary Material

Refer to Web version on PubMed Central for supplementary material.

Acknowledgments

This work was supported by a Canadian Institutes of Health Research (CIHR) Foundation grant (FDN-148366) to JP, and research grants from the NIH to JAP, Jr. (R35 GM118173, R24 GM-111625, R01 GM-067041) and to SV (R35 GM118078).

References

Abramson RD, Dever TE, Lawson TG, Ray BK, Thach RE, and Merrick WC (1987). The ATP-dependent interaction of eukaryotic initiation factors with mRNA. J Biol Chem 262, 3826–3832. [PubMed: 2950099]

Bhat M, Robichaud N, Hulea L, Sonenberg N, Pelletier J, and Topisirovic I (2015). Targeting the translation machinery in cancer. Nat Rev Drug Discov 14, 261–278. [PubMed: 25743081]

Bordeleau ME, Matthews J, Wojnar JM, Lindqvist L, Novac O, Jankowsky E, Sonenberg N, Northcote P, Teesdale-Spittle P, and Pelletier J (2005). Stimulation of mammalian translation initiation factor eIF4A activity by a small molecule inhibitor of eukaryotic translation. Proc Natl Acad Sci U S A 102, 10460–10465. [PubMed: 16030146]

Bordeleau ME, Robert F, Gerard B, Lindqvist L, Chen SM, Wendel HG, Brem B, Greger H, Lowe SW, Porco JA Jr., et al. (2008). Therapeutic suppression of translation initiation modulates chemosensitivity in a mouse lymphoma model. J Clin Invest 118, 2651–2660. [PubMed: 18551192]

Boussemart L, Malka-Mahieu H, Girault I, Allard D, Hemmingsson O, Tomasic G, Thomas M, Basmadjian C, Ribeiro N, Thuaud F, et al. (2014). eIF4F is a nexus of resistance to anti-BRAF and anti-MEK cancer therapies. Nature 513, 105–109. [PubMed: 25079330]

Chen ZH, Qi JJ, Wu QN, Lu JH, Liu ZX, Wang Y, Hu PS, Li T, Lin JF, Wu XY, et al. (2019). Eukaryotic initiation factor 4A2 promotes experimental metastasis and oxaliplatin resistance in colorectal cancer. Journal of experimental & clinical cancer research : CR 38, 196. [PubMed: 31088567]

Chu J, Galicia-Vazquez G, Cencic R, Mills JR, Katigbak A, Porco JA Jr., and Pelletier J (2016). CRISPR-Mediated Drug-Target Validation Reveals Selective Pharmacological Inhibition of the RNA Helicase, eIF4A. Cell Rep 15, 2340–2347. [PubMed: 27239032]

Ebada SS, Lajkiewicz N, Porco JA Jr., Li-Weber M, and Proksch P (2011). Chemistry and biology of rocaglamides (= flavaglines) and related derivatives from aglaia species (meliaceae). Prog Chem Org Nat Prod 94, 1–58. [PubMed: 21833837]

Galicia-Vazquez G, Cencic R, Robert F, Agenor AQ, and Pelletier J (2012). A cellular response linking eIF4AI activity to eIF4AII transcription. RNA 18, 1373–1384. [PubMed: 22589333]

Iwasaki S, Floor SN, and Ingolia NT (2016). Rocaglates convert DEAD-box protein eIF4A into a sequence-selective translational repressor. Nature 534, 558–561. [PubMed: 27309803]

Iwasaki S, Iwasaki W, Takahashi M, Sakamoto A, Watanabe C, Shichino Y, Floor SN, Fujiwara K, Mito M, Dodo K, et al. (2019). The Translation Inhibitor Rocaglamide Targets a Bimolecular Cavity between eIF4A and Polypurine RNA. Mol Cell 73, 738–748 e739. [PubMed: 30595437]

King ML, Chiang C-C, Limng H-C, Fujita E, Ochiai M, and McPhail AT (1982). X-Ray Crystal Structure of Rocaglamide, a Novel Antileukemic I H-Cyclopenta[b] benzofuran from Aglaia elliptifolia. J Chem Sco Chem Commun 20, 1150–1151.

Nielsen PJ, and Trachsel H (1988). The mouse protein synthesis initiation factor 4A gene family includes two related functional genes which are differentially expressed. EMBO J 7, 2097–2105. [PubMed: 3046931]

Novac O, Guenier AS, and Pelletier J (2004). Inhibitors of protein synthesis identified by a high throughput multiplexed translation screen. Nucleic Acids Res 32, 902–915. [PubMed: 14769948]

Pan L, Woodard JL, Lucas DM, Fuchs JR, and Kinghorn AD (2014). Rocaglamide, silvestrol and structurally related bioactive compounds from Aglaia species. Nat Prod Rep 31, 924–939. [PubMed: 24788392]

Pelletier J, and Sonenberg N (2019). The Organizing Principles of Eukaryotic Ribosome Recruitment. Annu Rev Biochem 88, 307–335. [PubMed: 31220979]

Qian Z, Hussein A-H, and Laurent D (2016). Recent Advances in the Synthesis of Flavaglines, a Family of Potent Bioactive Natural Compounds Originating from Traditional Chinese Medicine. Eur J Org Chem 2016, 5908–5916.

Ribeiro N, Thuaud F, Nebigil C, and Desaubry L (2012). Recent advances in the biology and chemistry of the flavaglines. Bioorg Med Chem 20, 1857–1864. [PubMed: 22071525]

Robert F, Roman W, Bramoulle A, Fellmann C, Roulston A, Shustik C, Porco JA Jr., Shore GC, Sebag M, and Pelletier J (2014). Translation initiation factor eIF4F modifies the dexamethasone response in multiple myeloma. Proc Natl Acad Sci U S A 111, 13421–13426. [PubMed: 25197055]

Roche SP, Cencic R, Pelletier J, and Porco JA Jr. (2010). Biomimetic photocycloaddition of 3-hydroxyflavones: synthesis and evaluation of rocaglate derivatives as inhibitors of eukaryotic translation. Angew Chem Int Ed Engl 49, 6533–6538. [PubMed: 20687060]

Rodrigo CM, Cencic R, Roche SP, Pelletier J, and Porco JA (2012). Synthesis of rocaglamide hydroxamates and related compounds as eukaryotic translation inhibitors: synthetic and biological studies. J Med Chem 55, 558–562. [PubMed: 22128783]

Rogers GW Jr., Komar AA, and Merrick WC (2002). eIF4A: the godfather of the DEAD box helicases. Prog Nucleic Acid Res Mol Biol 72, 307–331. [PubMed: 12206455]

Sokabe M, and Fraser CS (2017). A helicase-independent activity of eIF4A in promoting mRNA recruitment to the human ribosome. Proc Natl Acad Sci U S A 114, 6304–6309. [PubMed: 28559306]

Svitkin YV, Pause A, Haghighat A, Pyronnet S, Witherell G, Belsham GJ, and Sonenberg N (2001). The requirement for eukaryotic initiation factor 4A (elF4A) in translation is in direct proportion to the degree of mRNA 5' secondary structure. RNA 7, 382–394. [PubMed: 11333019]

Tecle H, Shao J, Li Y, Kothe M, Kazmirski S, Penzotti J, Ding YH, Ohren J, Moshinsky D, Coli R, et al. (2009). Beyond the MEK-pocket: can current MEK kinase inhibitors be utilized to synthesize novel type III NCKIs? Does the MEK-pocket exist in kinases other than MEK? Bioorg Med Chem Lett 19, 226–229. [PubMed: 19019675]

Wendel HG, De Stanchina E, Fridman JS, Malina A, Ray S, Kogan S, Cordon-Cardo C, Pelletier J, and Lowe SW (2004). Survival signalling by Akt and eIF4E in oncogenesis and cancer therapy. Nature 428, 332–337. [PubMed: 15029198]

Wolfe AL, Singh K, Zhong Y, Drewe P, Rajasekhar VK, Sanghvi VR, Mavrakis KJ, Jiang M, Roderick JE, Van der Meulen J, et al. (2014). RNA G-quadruplexes cause eIF4A-dependent oncogene translation in cancer. Nature 513, 65–70. [PubMed: 25079319]

Yoder-Hill J, Pause A, Sonenberg N, and Merrick WC (1993). The p46 subunit of eukaryotic initiation factor (eIF)-4F exchanges with eIF-4A. J Biol Chem 268, 5566–5573. [PubMed: 8449919]

Zhang W, Chu J, Cyr AM, Yueh H, Brown LE, Wang TT, Pelletier J, and Porco JA (2019). Intercepted Retro-Nazarov Reaction: Syntheses of Amidino-Rocaglate Derivatives and Their Biological Evaluation as eIF4A Inhibitors. J Am Chem Soc 10.1021/jacs.9b06446.

Significance.

The ability of rocaglates to function as interfacial inhibitors offers an opportunity by which to identify additional functional family members. Given the keen interest in this class of compounds as well as their target, we characterized the RNA binding specificity of eIF4A1 and eIF4A2 and found that both are quite similar in sequence preference and in their response to rocaglates. A screen of >200 rocaglates identified amidino-rocaglates – a potent chemical series extending knowledge on the structure-activity relationship of these compounds.

Highlights

- A screen of > 200 rocaglates for stimulation of eIF4A1:RNA clamping was prosecuted.
- eIF4A1 and eIF4A2 are similarly affected by all active rocaglates.
- Amidino-rocaglates were identified as a novel potent class of translation inhibitors
- A novel lead compound, CMLD012612, was identified and characterized

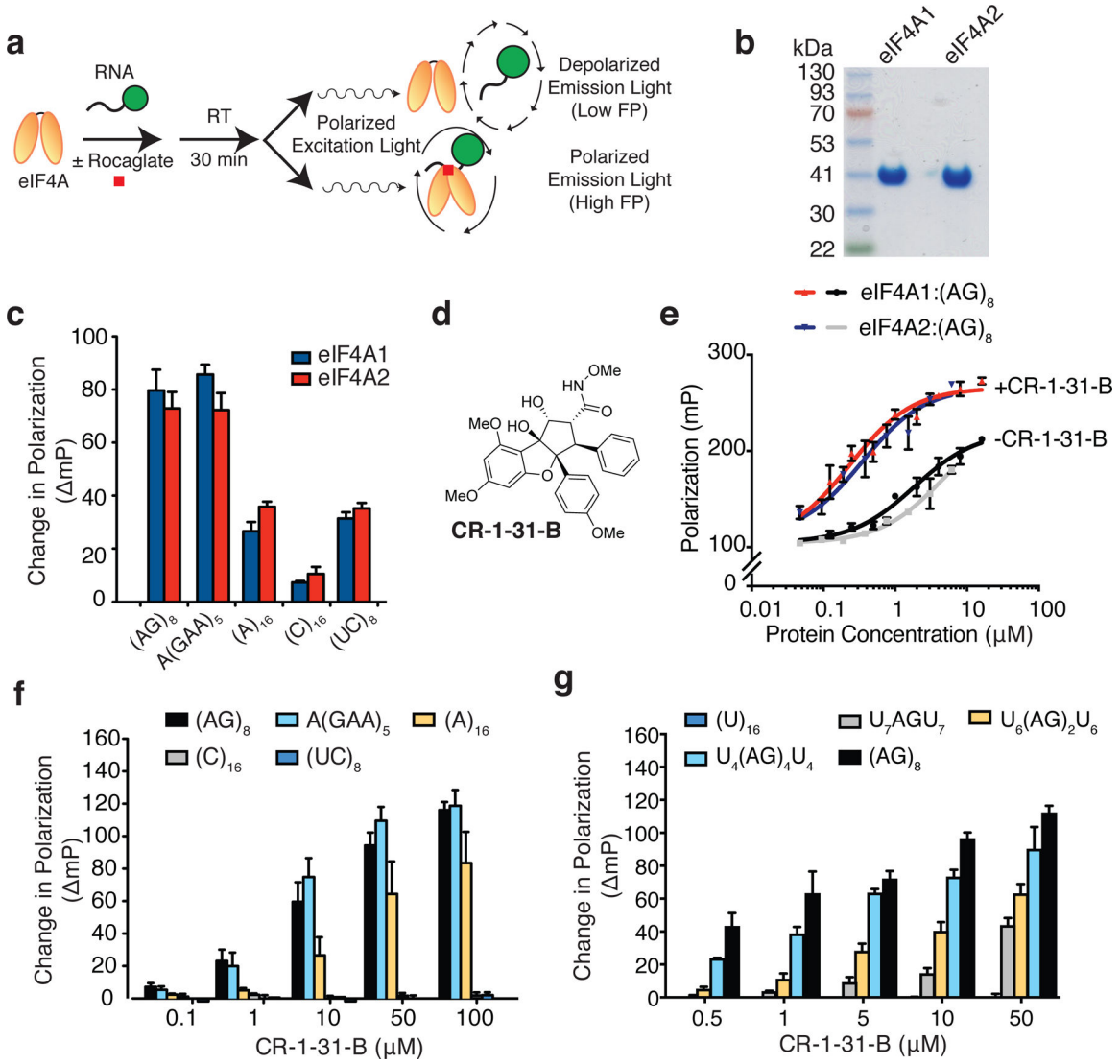

Figure 1. Rocaglates similarly enhance RNA binding of eIF4A1 and eIF4A2.

a. Schematic diagram of FP assay used to measure eIF4A:RNA association. FAM-labeled RNA probes are excited by plane-polarized light in the presence of eIF4A ± rocaglate. In the absence of eIF4A binding, the RNA probe rapidly tumbles and the emitted light becomes depolarized. Binding of eIF4A to RNA hinders probe rotation and results in polarized light emission. **b.** Coomassie blue staining of SDS-PAGE showing eIF4A1 and eIF4A2 preparations used herein. **c.** eIF4A1 and eIF4A2 possess similar RNA binding specificities. eIF4A1 or eIF4A2 (500 nM) were incubated in the presence of FAM-labelled RNA (10 nM) having the indicated sequence composition for 30 min, after which FP measurements were taken. The change in FP obtained relative to the DMSO control (which represents the eIF4A1:RNA association in the absence of compound) is presented. n = 3 ± SEM. **d.** Chemical structure of CR-1–31-B. **e.** Binding of eIF4A1 and eIF4A2 to RNA is equally responsive to CR-1–31-B. FAM labeled poly r(AG)$_8$ (10 nM) was mixed with the indicated concentrations of eIF4A1 or eIF4A2 either in the presence of vehicle (DMSO) or 10 μM CR-1–31-B. Reactions were equilibrated at RT for 30 min prior to measuring light

polarization. n = 3 ± SEM. **f.** Stimulation of eIF4A1:RNA binding by CR-1–31-B shows preference for polypurine-enriched sequences. FAM-labelled RNA was incubated in the presence of 500 nM eIF4A1 and the indicated concentration of CR-1–31-B for 30 min, after which time FP measurements were obtained. The change in FP relative to vehicle controls is presented. n = 3 ± SEM. **g.** The extent of eIF4A1:RNA binding stimulated by CR-1–31-B scales with polypurine content. FAM-labelled RNA was incubated with 500 nM eIF4A1 and the indicated concentration of CR-1–31-B for 30 min, after which time FP measurements were obtained. The change in FP obtained relative to vehicle controls is presented. n = 3 ± SEM.

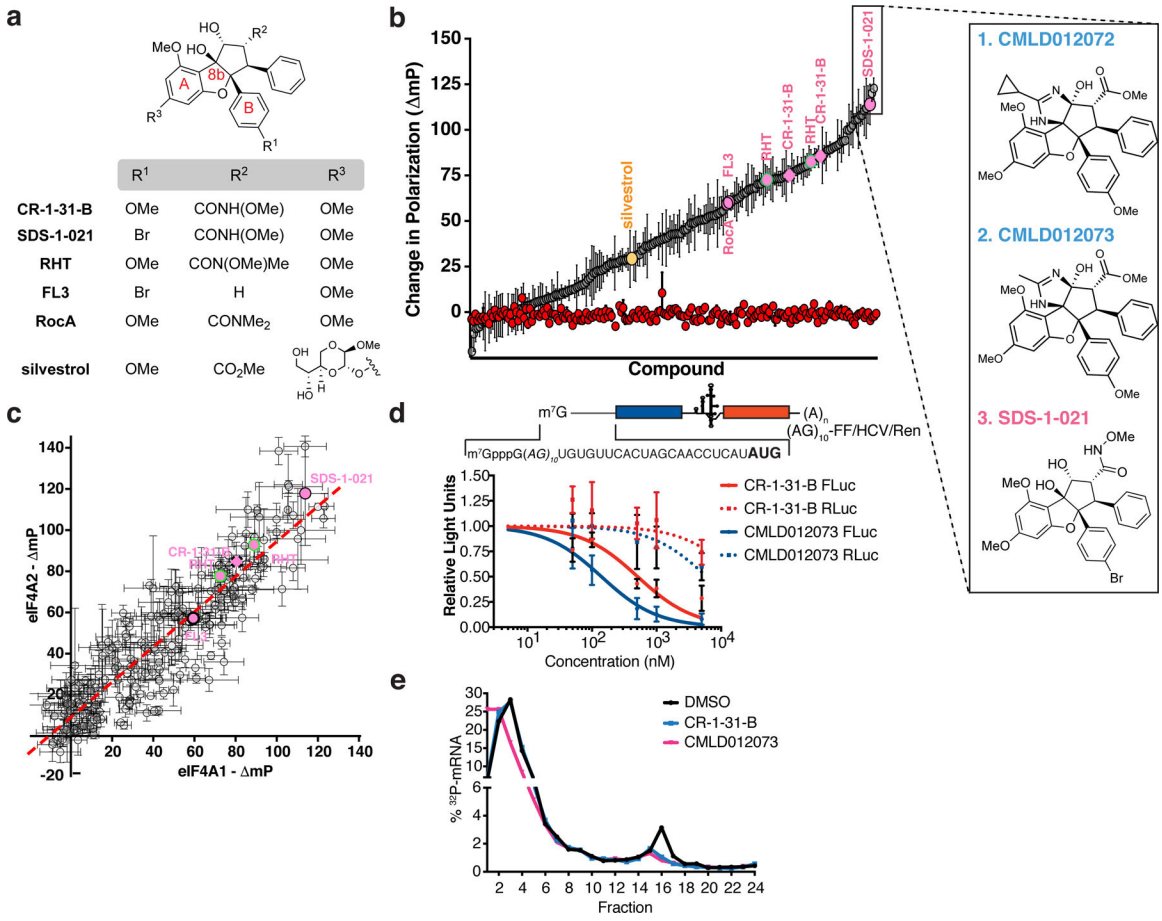

Figure 2. Rocaglate activity profiling.

a. Chemical structure of the most commonly used rocaglates in biological studies. **b.** Assessing eIF4A1:poly r(AG)$_8$ (grey circles) or eIF4A1:poly r(UC)$_8$ (red circles) RNA binding by FP in the presence of 10 μM rocaglate. Values are expressed relative to the DMSO control (containing RNA and protein in the absence of compound) and data is rank ordered. n = 3 ± SEM. Expanded view to the right shows the structures of the top three rocaglate hits. The duplication of RHT and CR-1–31-B represent independent compound preparations of different enantiomeric composition (see Table S1, column I for more details). **c.** Change in polarization obtained with eIF4A1:poly r(AG)$_8$ and eIF4A2:poly r(AG)$_8$ RNA. Pearson r = 0.814; p <0.0001. **d.** Inhibition of cap-dependent and independent translation (as reflected by firefly and renilla RLU, respectively) measured in response to compound in Krebs-2 extracts programmed with mRNA. n = 3 ± SEM. **e.** ^{32}P-labeled (AG)$_{10}$-FF/HCV/Ren mRNA was incubated with 100 nM eIF4A1 in the presence of 500 nM compound for 10 min at RT, then added to RRL in the presence of 600 μM cycloheximide. Complexes were resolved by sedimentation through a 10%–30% glycerol gradient.

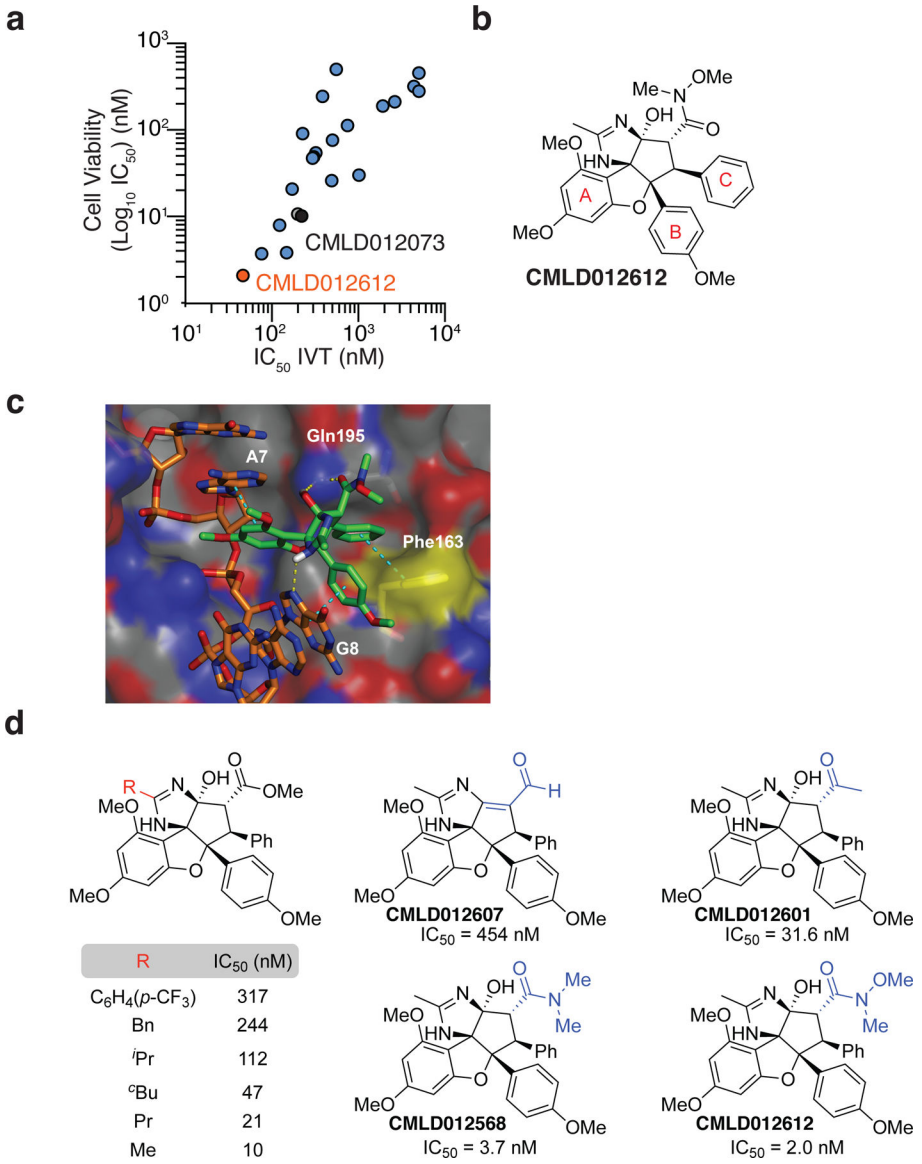

Figure 3. ADRs represent a potent class of rocaglates.

a. The IC_{50} for cytotoxicity against NIH/3T3 cells versus inhibition of *in vitro* translation is plotted for the ADR subfamily. Translation reactions were performed in RRL programmed with 10 ng/mL m^7GpppG-$(AG)_{10}$-FF/HCV/Ren. n = 3. See Table S2 for SEM values. Pearson r = 0.69, p <0.001. **b.** Structure of CMLD012612. **c.** Modeling of ADR CMLD012612 into the published X-ray structure of RocA in complex with eIF4A1 and poly-$(AG)_5$ RNA (PDB ID: 5ZC9). Hydrogen bonds are represented by a yellow line and **π**-stacking interactions are shown in cyan. **d.** SAR analysis of ADRs.

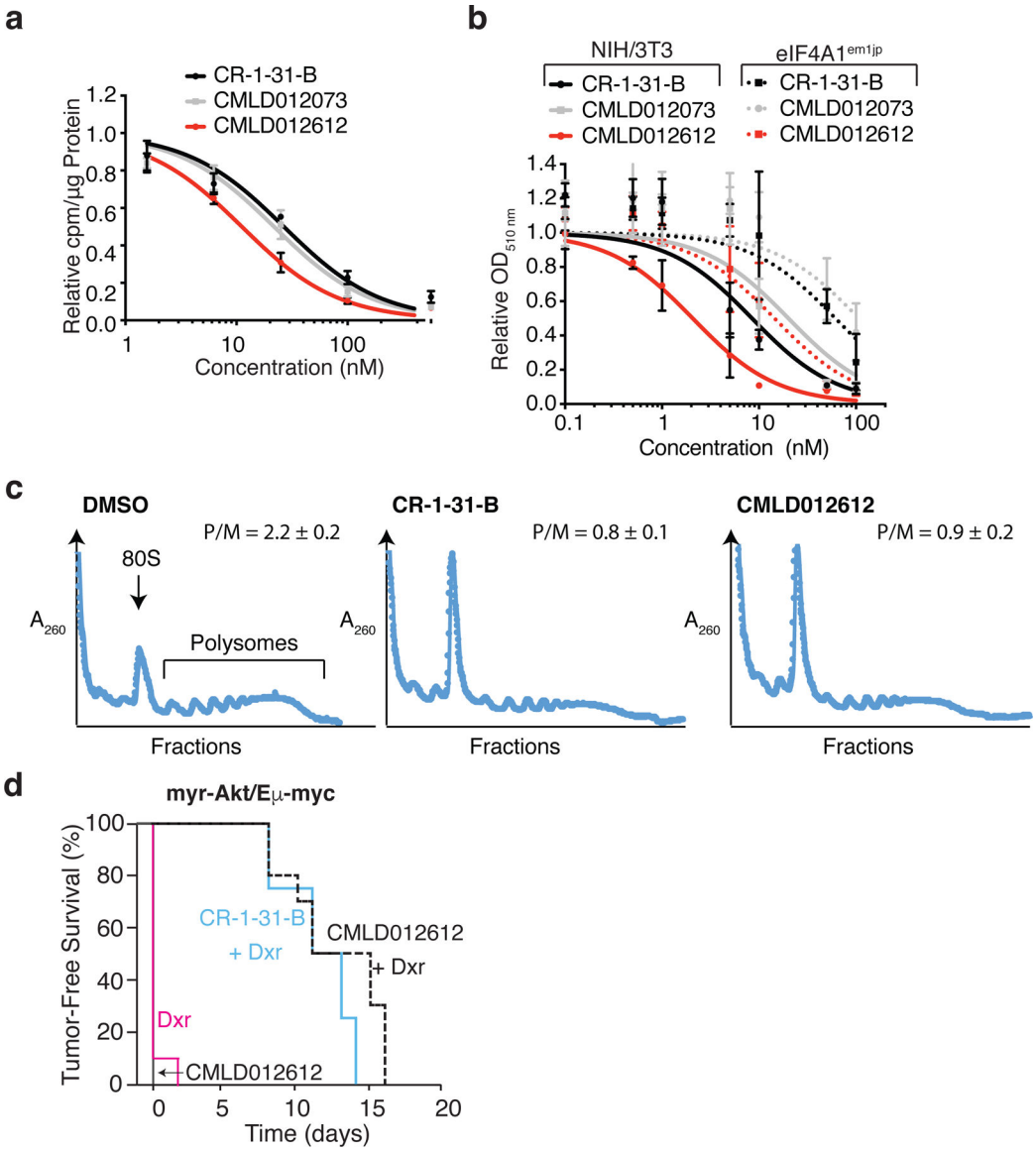

Figure 4. CMLD012612 inhibits tumor cell survival.

a. Inhibition of ^{35}S-methioinine incorporation in HEK293 cells following 1 h compound exposure. n = 3 ± SEM. **b.** Cytotoxicity of CMLD012612 towards NIH/3T3 and eIF4A1^{em1JP} cells following 4 day compound exposure. n = 3 ± SEM. **c.** CMLD012612 inhibits translation *in vivo* in the liver. Mice were injected with vehicle or CMLD012612 (0.5 mg/kg). Cytoplasmic extracts were prepared from livers 3 h later and resolved on 10%–50% sucrose gradients by centrifugation in an SW40 rotor at 150,000 × *g* for 2 h. Plotted are results of one representative experiment of two that showed similar results. The positions of 80S ribosomes and polysomes in the gradient are labeled, and the polysome/monosome (P/M) ratios indicated. **d.** CMLD012612 sensitizes myr-Akt/*E*μ-*Myc* tumors to doxorubicin *in vivo*. Kaplan-Meier plot showing tumor-free survival of mice bearing myr-Akt/*E*μ-*Myc* tumors following treatment with doxorubicin (Dox, red line; *n* = 10), CMLD012612 (solid black line; *n* = 10), CR-1–31-B + Dox (blue line; *n* = 4), or CMLD012612 + Dox (dashed

black line; $n = 10$). $p<0003$ for CR-1–31-B+Dox versus Dox, and $p<0.00001$ for CMLD012612+Dox versus Dox.